micromachines

MDPI

Article

Low-Stress and Optimum Design of Boost Converter for Renewable Energy Systems

Kashmala Salim [1], Muhammad Asif [2,*], Farman Ali [1], Ammar Armghan [3], Nasim Ullah [4,*], Al-Sharef Mohammad [4] and Ahmad Aziz Al Ahmadi [4]

[1] Department of Electrical Engineering, Qurtuba University of Science and IT, Dera Ismail Khan 29050, Pakistan; kashmalasaleem@qurtuba.edu.pk (K.S.); drfarmanali.optics@qurtuba.edu.pk (F.A.)
[2] Department of Electrical Engineering, Main Campus, University of Science & Technology, Bannu 28100, Pakistan
[3] Department of Electrical Engineering, College of Engineering, Jouf University, Sakaka 72388, Saudi Arabia; aarmghan@ju.edu.sa
[4] Department of Electrical Engineering, College of Engineering, Taif University, Al-Hawiyah P.O. Box 888, Saudi Arabia; m.alsharef@tu.edu.sa (A.-S.M.); aziz@tu.edu.sa (A.A.A.A.)
* Correspondence: masifeed@ustb.edu.pk (M.A.); nasimullah@tu.edu.sa (N.U.)

Abstract: This paper examines the design and analysis of DC–DC converters for high-power and low-voltage applications such as renewable energy sources (RESs) and comparisons between converters based on switch stresses and efficiency. The RESs including photovoltaic arrays and fuel cell stacks must have enhanced output voltages, such as 380 V DC in the case of a full bridge inverter or 760 V DC in the case of a half bridge inverter, in order to interface with the 220 V AC grid-connected power system. One of the primary difficulties in developing renewable energy systems is enhancing DC–DC converters' efficiency to enable high step-up voltage conversion with high efficiency and low voltage stress. In the present work, the efficiency, current, and voltage stress of switches of an isolated Flyback boost converter, simple DC–DC Boost converter, and an Interleaved boost converter, are explored and studied relatively. The most suitable and optimized options with a high efficiency and low switching stress are investigated. The more suitable topology is designed and analyzed for the switch technology based on the Silicon-Metal Oxide Semiconductor Field Effect Transistor (Si-MOSFET) and the Gallium Nitride-High Electron Mobility Transistor (GaN-HEMT). The Analytical approach is analyzed in this paper based on efficiency and switching stress. It is explored that GaN HEMT based Flyback boost converter is the best. Finally, the future direction for further improving the efficiency of the proposed boost converter is investigated.

Keywords: DC–DC converters; Flyback boost converter using Si-MOSFET switch technology; Flyback boost converter using GaN-HEMT switch technology

Citation: Salim, K.; Asif, M.; Ali, F.; Armghan, A.; Ullah, N.; Mohammad, A.-S.; Al Ahmadi, A.A. Low-Stress and Optimum Design of Boost Converter for Renewable Energy Systems. *Micromachines* **2022**, *13*, 1085. https://doi.org/10.3390/mi13071085

Academic Editors: Chun-An Cheng, Hung-Liang Cheng, En-Chih Chang, Chien-Hsuan Chang and Ching-Min Lee

Received: 13 June 2022
Accepted: 5 July 2022
Published: 8 July 2022

1. Introduction

Recently, there has been a continuous increase in environmental issues. As a result, retardations have occurred in the power generation based on fossil fuel [1,2]. In addition, the rapid growth of energy consumption across the globe has increased numerous renewable energy-based power generation systems, control algorithms, smart grids, advanced energy conversion, hybrid energy storage systems, and management systems. These systems require advanced power converters to convert the voltage efficiently; as a result, the power generation based on renewable energy sources will be enhanced [3,4]. Therefore, recently, power generation through improved control techniques and better power switching devices is one of the hot research areas [5,6]. One of the main concerns is that renewable energy sources have a low Direct Current (DC) output voltage, such as fuel cell stacks and photovoltaic arrays. It is important to increase the range of voltage to the next level,

e.g., 380 V DC in the case of the inverter (full bridge) and 760.00 V-DC in the case of the inverter (half bridge) for yielding 220 V AC output to be interfaced with a grid-connected power system of 220 V AC [7]. DC-to-DC converter development for delivering a high step-up voltage conversion with a low switch stress and high efficiency is one of the key challenges in advancing renewable energy systems [8]. Figure 1 shows the block diagram of a single-phase hybrid renewable energy grid-connected system. In general, such a system consists of a photovoltaic (PV) array, fuel cell stack, batteries, DC-to-DC converters, and inverter [9]. Those DC-to-DC converters with high step-up conversion ratios are needed to interface low-voltage outputs of fuel cell stacks and photovoltaic arrays, typically 22–48 V, with a relatively high-voltage (200+ V) DC link for supplying standalone or grid-connected AC loads through an inverter [10].

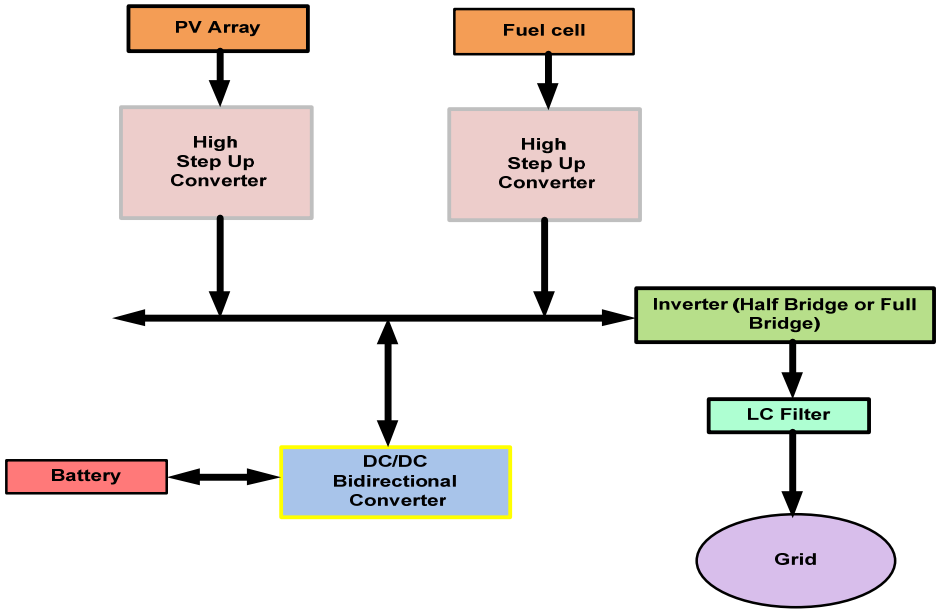

Figure 1. Block diagram of a hybrid renewable energy grid-connected system.

To assist this growth trend and attain the required performance of the system, the development of enhanced power converters with improved control algorithms and switching devices is essential. Furthermore, the need for communication capability, improvement in the power level, and performance of the converters system are also assessed to have a rapid growth to assist enhancement in the present technologies. Therefore, to realize the above aims, it is essential to consider advanced semiconductor switching features, e.g., lower switching losses, high switching frequency, smaller sizes, thermal capability, and higher power densities.

To obtain the above stated quality standards and application goals, gallium nitride (GaN)-based High Electron Mobility Transistor (HEMT) (wide-bandgap) and Silicon-Metal Oxide Semiconductor Field Effect Transistor (SiC-based MOSFET) are commonly referred to in this paper as the best switching devices [11–14]. This research focuses on studying several DC-to-DC boost converters in terms of their suitability to be used in such power systems.

Related Work

Researchers have examined various converters to discover converters that give greater voltage conversion ratios with a step-up property, higher efficiency, and lower stresses of switch voltage. There are numerous DC–DC boost converters in the market; however, by reasons of high cost and complex structures, unnecessary auxiliary circuits, parasitic ringing issues, and high power consumptions, these converters cannot be recommended for renewable energy systems. The type of isolated converters can upsurge the system's structure and expense while increasing losses. [15] proposes a novel interleaved boost

converter for Uninterruptible Power Supply (UPS) applications having a high Voltage Conversion Ratio (VCR). The converter employs a magnetically connected circuit similar to that of a traditional converter. Reference [16] proposes a converter with a single stage for a power generation system based on the PV. This work has explored the importance of such a converter when a lower efficiency and reliability, higher dimensions and cost, and parts are the main targets. This type of converter enhances the solar arrays' relatively low voltage and converts input DC electricity to generate AC power with better quality to be faded to the grid. In this case, the highest quantity of power will be taken out from the PV array. In [17], the authors have suggested a stage-shift-controlled three-stage, transformer-secluded DC-to-DC converter for fuel cells with lower voltages. On the source side, the converter greatly raises the voltage. It runs at 240 amperes, creating the strategy of a DC–DC converter with a higher current and lower voltage extremely difficult, reduced transformer turns ratio by keeping the voltage constant and decreasing dimensions of inactive components, e.g., the filter capacitor that is used at the output and bus capacitor that is used at the input. Normally the above concept is applied in three interleaving phases for organizing loads, eradicating the ripple current of the inductor at angles having a shift of larger than one hundred twenty degrees and Zero-Voltage–Zero-Current (ZVZC) switches. In [18–20], a group of DC-to-DC converters is discussed with a simple topology having high efficiencies. The suggested converters based on coupled winding and diode perform better than their counterparts, i.e., active-clamp. By recycling leakage energy and alleviating the reverse recovery issue, better efficiency is achieved. Wide bandgap devices are game-changing power electronics technology for high-efficiency and high-frequency applications. In [21], the authors have discussed a DC-to-DC boost converter topology that integrates the properties of the interleaved set up. For this purpose, a 100 W prototype converter is suggested with a PIC16F microcontroller.

For low- and high-output voltage applications, a DC-to-DC boost converter topology was presented in [22] using two hybrid voltage multiple cells, a single switch, and three winding couple inductors. In [23], the authors discussed a hybrid non-isolated DC–DC commutation cell and derived three different DC–DC converters, a buck-type, a boost-type, and a buck-boost-type, which is generated by the integration between a conventional commutation cell and ladder-type passive switched capacitor (SC). A cell 1 kW prototype was developed to verify the operation of the three proposed converters. To maintain the output voltage of DC-to-DC inverting buck boost power converter operation, the authors have presented a novel Lyapunov function=based robust nonlinear proportional integral controller in [24]. The paper [25], discusses the quadratic Lyapunov function for the classical two-level converters and two switching control designing.

2. Proposed and Analytical Modeling

The performance and investigation of DC–DC converters, i.e., interleaved boost converter, Flyback-based converter, and simple boost converter, are briefly demonstrated as shown in Figure 2. The analysis of DC–DC converters means to derive expressions for the inductor currents, output, and capacitor voltages of the targeted converters by applying two different techniques, i.e., capacitor charge balance and inductor volt–second balance [26]. Flyback-based and interleaved boost converters were analyzed for different switching modes. Two input levels, an associated transformer, current-fed input circuits, and a subsidiary rectifier bridge make up the converter. Each input-stage course has two control switches (power) and two inductors. To allow for the overlapping process, the values of Q1 and Q4 switches should be higher than 0.5 in order to achieve smooth conversions. These can be mathematically expressed [27] as the following.

$$\phi = D\ Ts - \frac{Ts}{2} \tag{1}$$

$$\phi = (2D - 1)\ \frac{Ts}{2} \tag{2}$$

In the above equations, D is duty ratio, ϕ is the phase of the waveform, and Ts is the period of switching.

Actually, D denotes the Pulse Width Modulation (PWM) generator's duty cycle, whereas Ts denotes the switching period. There are always four operational modes during the switching time.

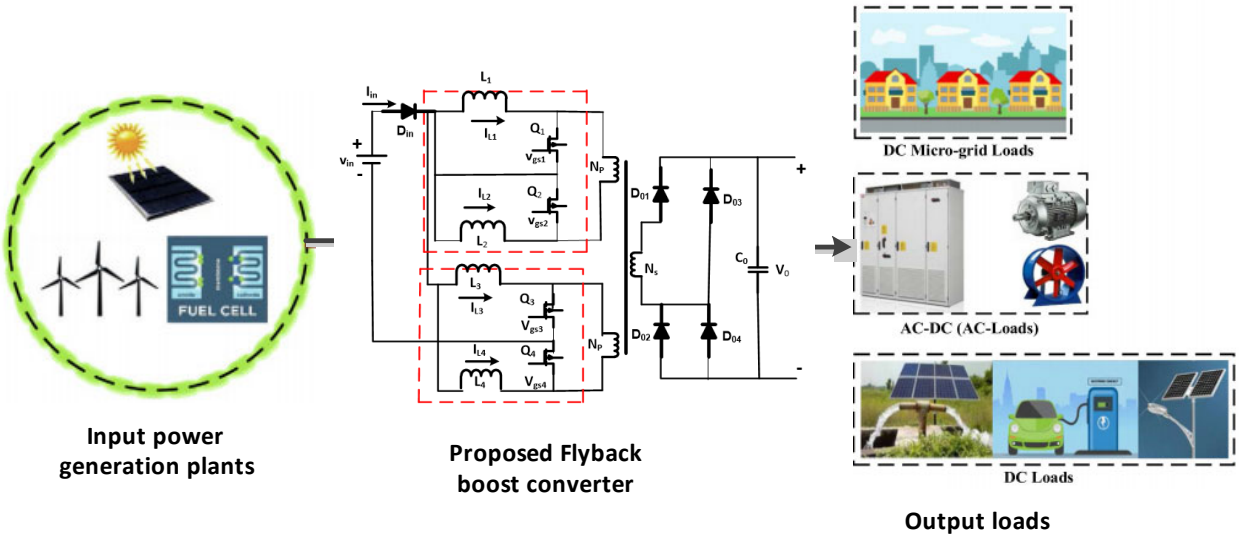

Figure 2. Proposed Flyback-based converter.

2.1. First Mode (t0–t1)

MOSFETs Q1 and Q3 are turned on in Mode 1, whereas Q2 and Q4 are off. MOSFETs Q1 and Q3 carry the currents inductors i_{L1} and i_{L3}, respectively. As Figure 3 depicts, the currents of inductors i_{L2} and i_{L4} drift into the windings of the transformer, i.e., first and second primary, respectively. The following equations give the voltage of inductors v_{L4}, v_{L3}, v_{L2}, and v_{L1} as well as the current of inductors i_{L4}, i_{L3}, i_{L2}, and i_{L1} [28–30]:

$$v_{L2} = v_{in} - P_{rimary} \tag{3}$$

$$v_{L4} = v_{in} - n \times V_0 \tag{4}$$

$$i_{L1} = i_{L1}(t_0) + \frac{(v_{in} \times t - t_0)}{L} \tag{5}$$

$$i_{L\_2} = i_{L2}(t_0) - \frac{(n \times Vo - Vin) \times (t - t0)}{L1} \tag{6}$$

$$i_{L\_3} = i_{L3}(t_01) - \frac{(v_{in}) \times (t - t_0)}{L} \tag{7}$$

$$i_{L\_4} = i_{L4}(t_01) - \frac{(n \times Vo - Vin) \times (t - t0)}{L} \tag{8}$$

L stands for the inductance of inductors L_1 to L_4, and n stands for the transformer's rotation ratio. Lin's source current is equal to the sum of the inductor currents i_{L1} to i_{L4}. This is noted that in the inductors, current i_{L3} and i_{L1} growth is rectilinear. In contrast, the waveforms of inductor currents i_{L2} and i_{L4} reduction are linear when the inductor current behavior is studied in Figure 3. This cancels the source current's ripple, which is desired, especially for generating lower-voltage and power, e.g., stacked fuel cells and solar arrays. Diodes D03 and D02 transmit the energy towards the load in the case of Mode 1.

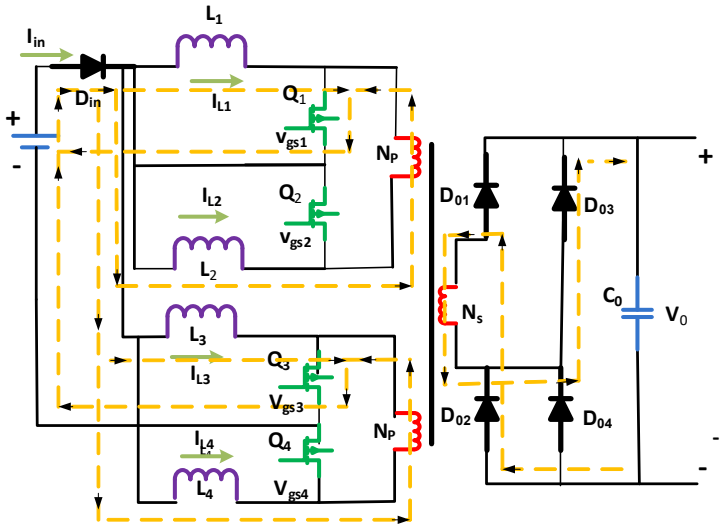

Figure 3. First mode of the circuit.

2.2. Second Mode (t1–t2)

The four MOSFETs Q4, Q1, Q2, and Q3 are optimized in Mode 2 as mentioned in Figure 4. Soft switching turns on MOSFETs Q2 and Q4 at time *t*1. The current of the inductors goes down/declines a little before time *t*1. Initially, the inductance leakage transformer tries to oppose the current flow for a while, and the output capacitor of Q2 begins to discharge. As a result, switch Q2 appears to be short-circuited.

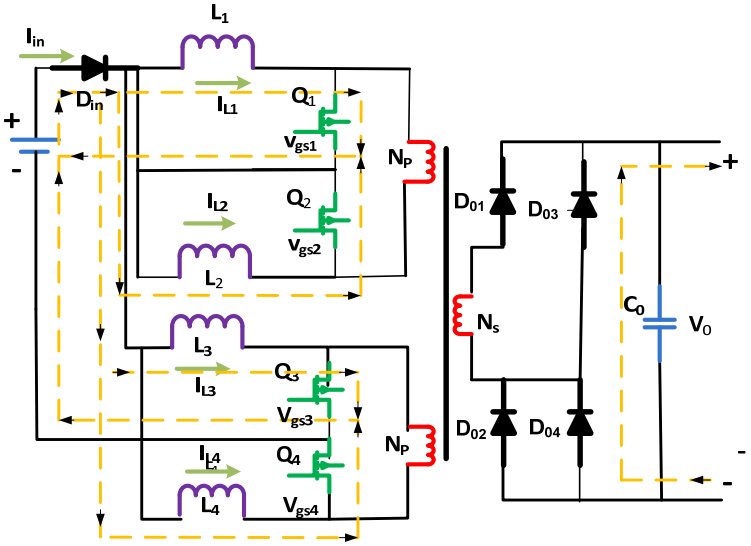

Figure 4. Second mode of the circuit.

The transformer's leakage inductance is chosen; for example, it opposes the switch current for a short moment so that the draft of the switch approaches its highest rate; or else, Q2 would not switch to zero voltage. The number four, i.e., MOSFET Q4, could also be optimized by applying Zero Voltage Switching (ZVS). To accomplish ZVS, power devices should fulfill the below condition:

$$\frac{I_{in}}{4} \geq \frac{nV_0}{L_{lk}} \times t_r(\text{max.}) \tag{9}$$

In the above equation, *tr* (max.) shows the maximum time for the rise of the switch's current. At the same time, L_{lk} shows the transformer's primary winding leakage. During this time, all electrical switches are turned on.

Similarly, the switches three Q3 and four Q4 of the MOSFETs carry inductor currents i_{L3} and i_{L4}, respectively. Inductor currents i_{L1} to i_{L4} grow linearly over this period. The following equations give the voltages of the inductor v_{L4}, v_{L1}, v_{L2}, and v_{L3}, as well as the currents of inductors i_{L4}, i_{L3}, i_{L2}, and i_{L1}:

$$v_{L1} = v_{in} \tag{10}$$

$$v_{L2} = v_{in} \tag{11}$$

$$v_{L3} = v_{in} \tag{12}$$

$$v_{L4} = v_{in} \tag{13}$$

$$i_{L1} = i_{L1}(t_1) + \frac{(v_{in} \times t - t_1)}{L} \tag{14}$$

$$i_{L2} = i_{L2}(t_1) - \frac{(n \times Vo - Vin) \times (t - t1)}{L} \tag{15}$$

$$i_{L3} = i_{L3}(t_1) - \frac{(v_{in}) \times (t - t_1)}{L} \tag{16}$$

$$i_{L4} = i_{L4}(t_1) - \frac{(n \times Vo - Vin) \times (t - t1)}{L} \tag{17}$$

Through the transformer, the stored energy is transferred towards the load using the first leakage inductances of the windings. The current (secondary) of the windings of the transformer flops to (0) zero after the stored energy is fully delivered. At this stage, the output of the diodes is disabled. The load is fed by the discharge of the output capacitor Co. The voltages that appear crosswise the two transformer's primary winding stay at (0) zero during this overlapping time ($t1$–$t2$). Zero voltage switching occurs once the switches Q3 and Q1 are switched off at the moment interval $t2$.

2.3. Third Mode (t2–t3)

MOSFETs Q1 and Q3 are switched off in this mode, whereas Q2 and Q4 are turned on. i_{L2} and i_{L4} inductor currents run through Q2 and Q4, respectively (Figure 5). The first and second primary transformer windings carry inductor currents i_{L1} and i_{L3}. The voltages of the inductors v_{L4}, v_{L1}, v_{L2}, and v_{L3}, as well as the currents of the inductors i_{L4}, i_{L2}, i_{L1}, and i_{L3}, are explained by the Equations during ($t2$–$t3$) [31–34]:

$$v_{L1} = v_{in} - P_{rimary} \tag{18}$$

$$v_{L2} = v_{in} \tag{19}$$

$$v_{L3} = v_{in} - n \times V_0 \tag{20}$$

$$v_{L4} = v_{in} \tag{21}$$

$$i_{L1} = i_{L1}(t_2) + \frac{(v_{in} \times t - t_2)}{L} \tag{22}$$

$$i_{L2} = i_{L2}(t_2) - \frac{(n \times Vo - Vin) \times (t - t2)}{L} \tag{23}$$

$$i_{L3} = i_{L3}(t_2) - \frac{(v_{in}) \times (t - t_2)}{L} \tag{24}$$

$$i_{L4} = i_{L4}(t_2) - \frac{(n \times Vo - Vin) \times (t - t2)}{L} \tag{25}$$

These equations reveal that throughout this interval, the currents of the inductors i_{L3} and i_{L1} reduce, while the currents of the inductors i_{L4} and i_{L3} grow smoothly. As a result, the source current's ripple is canceled. During this time, the rectifying diodes D4 and D1 transport energy to the load from the source.

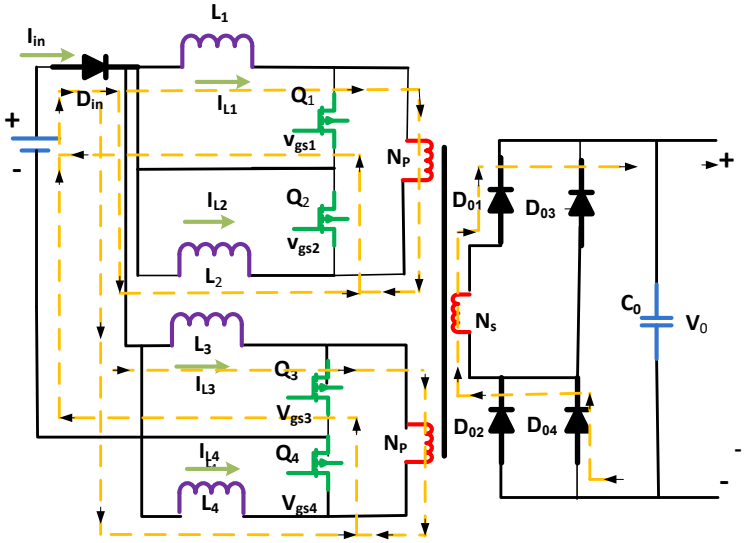

Figure 5. Third mode of the circuit.

2.4. Fourth Mode (t3–t4)

The four MOSFETs, Q4, Q2, Q3, and Q1, will be kept in on state in this mode as discussed in Figure 6. Soft switching is used to turn on MOSFETs Q1 and Q3. The operation of the circuit is identical to that of Mode 2. The inductor currents i_{L1} to i_{L4} rise in a linear fashion. The following equations give the voltage of the inductors v_{L4}, v_{L2}, v_{L3}, and v_{L1}, as well as the current of the inductor i_{L4}, i_{L2}, i_{L3}, and i_{L1} [35]:

$$v_{L1} = v_{in} \tag{26}$$

$$v_{L2} = v_{in} \tag{27}$$

$$v_{L3} = v_{in} \tag{28}$$

$$v_{L4} = v_{in} \tag{29}$$

$$i_{L1} = i_{L1}(t_4) + \frac{(v_{in} \times t - t_4)}{L} \tag{30}$$

$$i_{L2} = i_{L2}(t_4) - \frac{(n \times Vo - Vin) \times (t - t4)}{L} \tag{31}$$

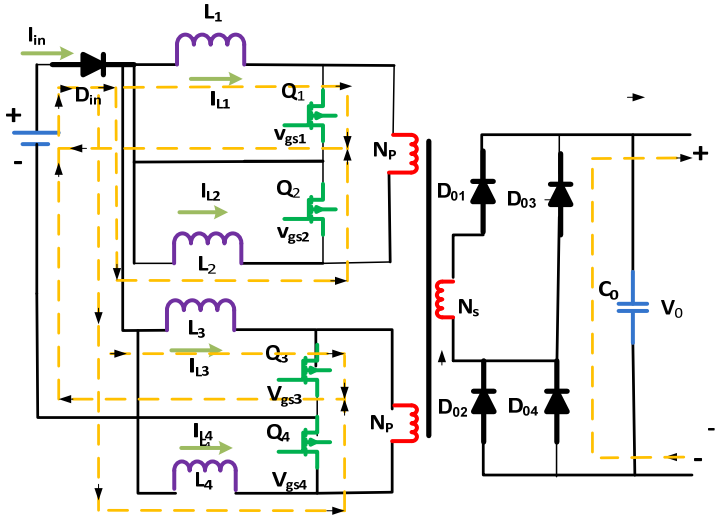

Figure 6. Fourth mode of the circuit.

The leakage inductance stores the energy in the two-primary winding of the transformer. This energy is then transmitted from the *Tx* to the load. The current that is called the secondary current of the *Tx* flops to "0" when the overall of the stored energy is delivered. Altogether, the diodes called the secondary rectifying diodes are disabled, and the output capacitor is used only to feed the load. The voltages that appear crosswise the two-primary winding of the transformer continue to be zero over the period ($t3$–$t4$). Soft switching is achieved when MOSFETs Q2 and Q4 turn off at time $t4$. After one interval, *Ts*, the circuit changes back to Mode 1.

3. Current and Voltage Stresses of the Switches

The silicon area is reduced when overall switch stress is minimized. During Mode 1 and Mode 3, the peak voltage across switches is identical to the actual voltage of the transformer, which is the reflection of the voltage of the load. The stress can be expressed [36–40] as:

$$V_{stress} = nV_0 \tag{32}$$

During Mode 1 and Mode 3, the maximum current through a switch is given by:

$$I_{Stress} = I_{L1} = I_{L2} = I_{L3} = I_{L4} = \frac{I_{in}}{2} \tag{33}$$

As a result, the switches only carry 50 percent of the current source. Additionally, actually, it is especially essential in the case of the sources while dealing with lower voltages, for example, stacked fuel cells and modules of solar arrays. Normally, lower voltage sources deliver greater currents in the applications of greater power that necessitate high-current switches. The switch stress is calculated as follows:

$$S = V_{Stress} \times I_{Stress} \tag{34}$$

It is a good idea to compare the potential converter's overall switch stress and switch utilization. The voltages and currents put on semiconductor devices should be kept to a minimum in a good design. The following is how the total switch stress is calculated:

$$S = \sum_{i=1}^{k} V_i I_i \tag{35}$$

The k represents the actual number of devices (semiconductors). Additionally, the stress of the voltage of the first switch is defined by V_i, and I_i represents the Root Mean Square (RMS) value of the current of the first switch. The maximum amplitude of the wind is frequently referred to rather than the current RMS value. The overall stress of the switch stress can be calculated as follows:

$$S = 4\left(nV_0 \times \frac{I_{in}}{2}\right) \tag{36}$$

The switch utilization is defined as follows:

$$U = \frac{P_{load}}{S} \tag{37}$$

Switch use is kept high in a good converter design.

The efficiency and MOSFET/HEMT stresses of the converters are included in the simulation results. The parameters that are selected for designing the converters are specified below in Table 1.

Table 1. Parameters detail used for design converters.

Parameter	Description
Input power	1 kW
Input voltage	48 V
Input current	20.83 Amp
Output voltage	380 volts (for full bridge inverter)
Output current	2.63 Amp
Resistance	144.487 Ohm

The transformer's turn ratio of Flyback boost converter is computed as follows:

$$n = \frac{V_{in}}{V_0 \times (1 - D)} = 0.4 \tag{38}$$

Because there are two unknowns in the preceding equation, and it is essential to select a sufficient number for the other unknown before determining the value of the first, $D = 0.684110$ was used to permit overlap among the switches. The computation of the switches' current and voltage are presented below:

$$V_{Stress} = n \times V_0 = 152 \text{ Volt} \tag{39}$$

$$I_{Stress} = \frac{I_m}{2} = 10.415 \text{ A} \tag{40}$$

The peak-to-peak ripple has been set at thirty percent of the current of the inductor. The inductors inductances are determined in the following manner.

$$L = \frac{DV_m}{\Delta i_L \times f_s} = 0.14894 \times 10^3 \text{ H} \tag{41}$$

$$L \cong 210 \text{ uH} \tag{42}$$

The voltage ripple on the capacitor is set to 0.1 percent of the output voltage. The following is the value of capacitance C_0 when the ripple voltage is this:

$$C_0 = \frac{I_0 \times (1 - D)T_s}{\Delta V_0} = 21.85 \text{ uF} \tag{43}$$

The design parameters for the boost converter were chosen based on the supplied parameters. The detailed calculation of the duty ratio for a boost converter is presented here.

$$D = 1 - \frac{V_{in}}{V_0} = 0.874 \tag{44}$$

The switches' voltage and current ratings are as follows:

$$V_{Stress} = V_0 = 380 \text{ Volt} \tag{45}$$

$$I_{Stress} = I_m = 20.83 \text{ A} \tag{46}$$

Assume that the maximum ripples, denoted by i_L, are thirty percent of the current of the inductor. The inductance L is then determined as

$$L = \frac{V_{in} \times DT}{\Delta i_L} = 67 \text{ uH} \times 10^3 \text{ H} \tag{47}$$

Allow 0.1 percent of the output voltage for capacitor voltage ripple. The output capacitor's capacitance is then calculated as

$$C = \frac{V_0 \times DT}{\Delta v \times R} = 60.48 \text{ uF} \tag{48}$$

4. Results and Discussions

Flyback boost, simple boost, and interleaved boost converters were used for low-voltage, high-power renewable energy systems. These converters offer high step-up conversion ratios, high efficiencies, and low switch voltage stresses. They may produce a high output voltage from common voltage sources such as solar arrays and fuel cells. The output voltages and powers waveforms and switch currents and voltages waveforms of the three converters were obtained after successful converter circuit simulation in OrCAD PSpice. The goal was to prove which converter is superior for low-voltage high-power applications in terms of voltage conversion ratio, efficiency, and switch stresses. At the end of the article, Tables 1 and 2 summarize the simulated converters. Figure 7 depicts the output voltage waveform of the proposed Flyback boost converter. This waveform shows a voltage output of 371.583 V.

Table 2. Characteristics of Flyback boost, simple boost, and interleaved boost converters Si-MOSFET/GaN-HEMT.

S.NO	Parameter	Flyback-Based Converter (Si-MOSFET) (%)	Boost Converter (Si-MOSFET)	Interleaved Boost Converter (Si-MOSFET)	Flyback Boost Converter (GaN-HEMT)
1	Efficiency	95	93.5	91	97
2	Voltage Stress	151.28	364.68	362.98	150.001
3	Current Stress	10.402	26.02	7.6327	10.001

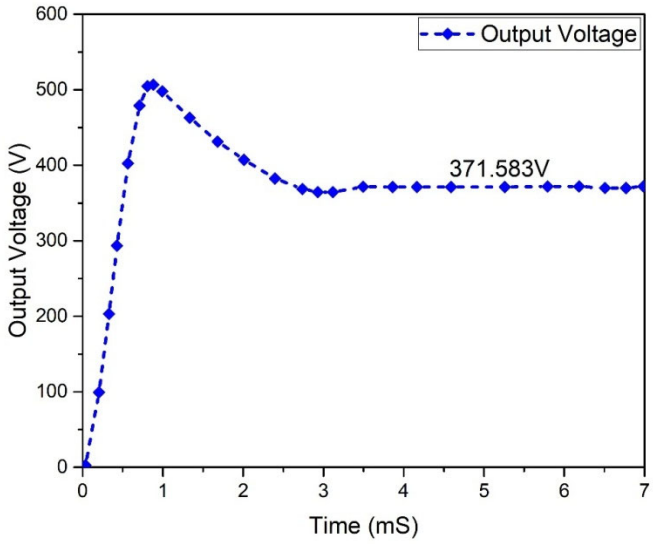

Figure 7. Flyback boost converter output voltage.

In two switching periods, the current of the inductor's behavior is studied concerning the gate signals of switches S2 and S1. It is the same current flowing through L1 or L3. It illustrates that after the switch S3/S1 is turned on, the current i_{L1}/i_{L3} increases and declines until S1/S3 are turned off again. The inductor current through L2 or L4 was studied, and it was found that its magnitude is the same as the current in L3 or L1. In two switching periods, the currents of inductors i_{L4}/i_{L2} were studied concerning the gate signals of switches S2 and S1. It was found that after the switch S2/S4 is made on, the current i_{L2}/i_{L4}

increases and then declines until S2/S4 is turned on again. The waveform/behavior of the input current of the Flyback boost converter is depicted in Figure 8 and reveals a current of 20.7 A. In one switching period, the input current and the inductor currents were studied and demonstrated how the input current ripple is decreased.

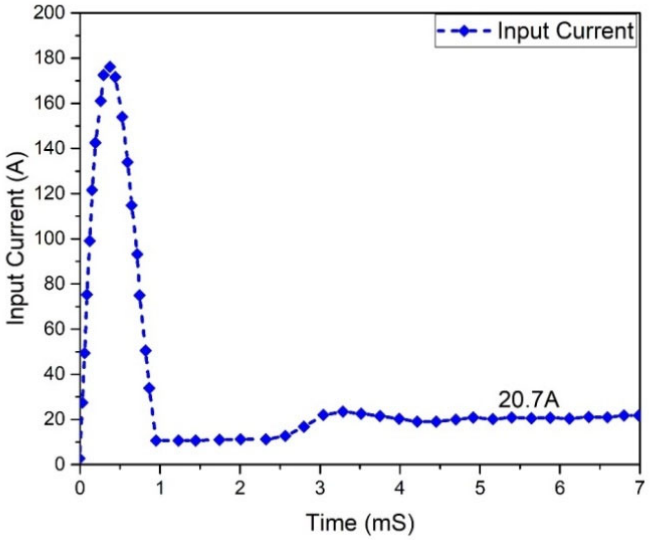

Figure 8. Input current analysis of Flyback boost converter.

The current of the Flyback boost converter that flows across the load is 2.57160 A, as shown in Figure 9. During one switching interval, the load current was also studied. The load, 70% current, was caused by energy delivered to the load via the transformer and through a pair of diodes. The discharge of the capacitor causes the current of the load via the load during the overlapping period. Since both MOSFETs in each current-fed input circuit were conducting throughout the overlapping period, there was no voltage across the transformer windings because no current was flowing through the transformer's primary windings.

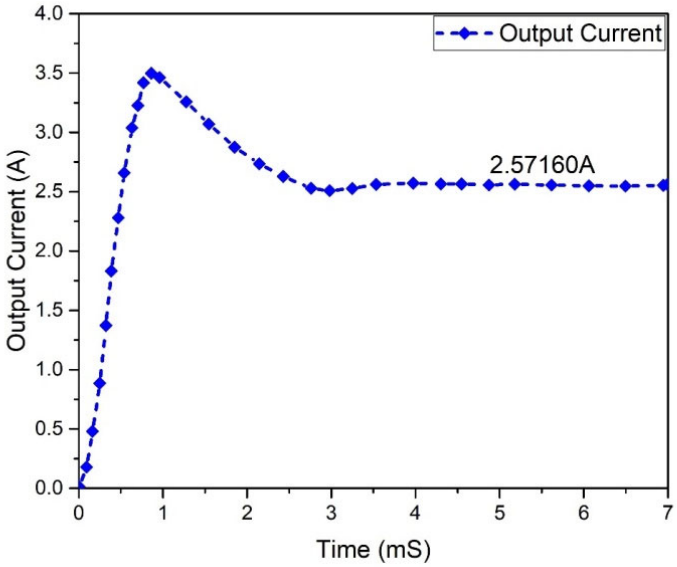

Figure 9. Flyback boost converter output current.

Input and output power graphs are shown in Figures 10 and 11. The graph behavior illustrates that the value of the output power was almost 0.950555 W, while the input power value was 1 kW.

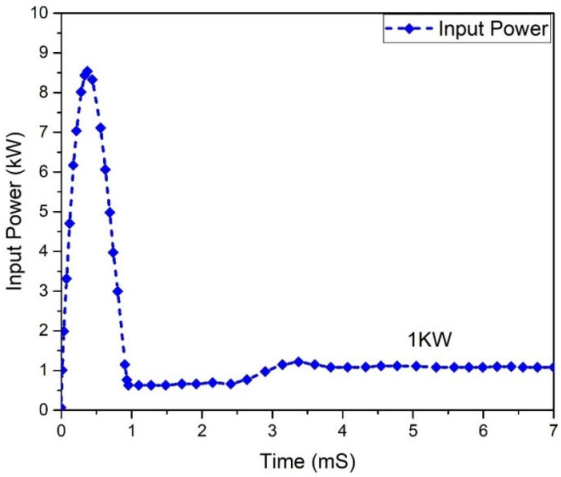

Figure 10. Input power analysis of Flyback boost converter.

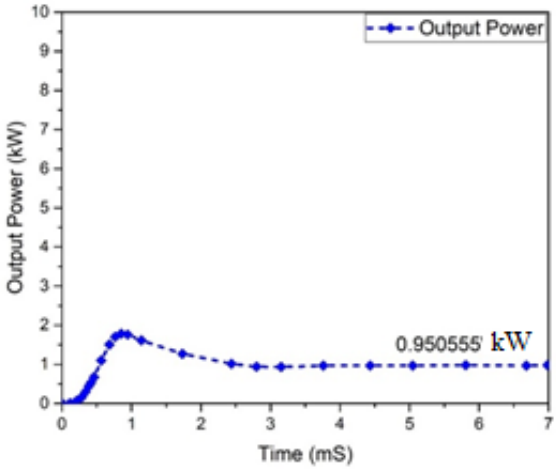

Figure 11. Output power of Flyback boost converter.

The graphs of the current and voltage behavior of the boost converter are examined in Figures 12 and 13, which show the 362.293 V and 2.50801 A output voltage and current, respectively. The output and input power waveforms are revealed in Figures 14 and 15, respectively. Figure 14 shows the output power of 908.932 W, whereas Figure 15 depicts the input power of 1 KW.

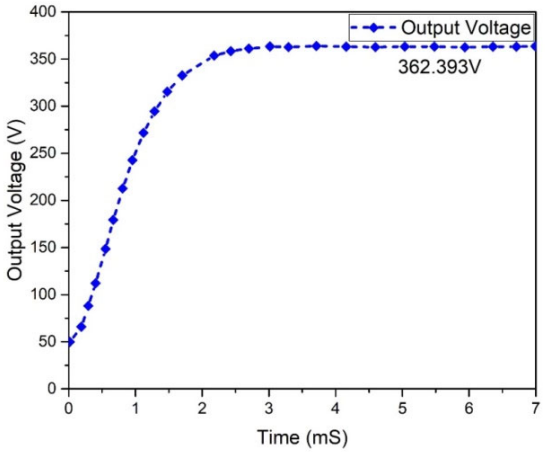

Figure 12. Boost converter output voltage.

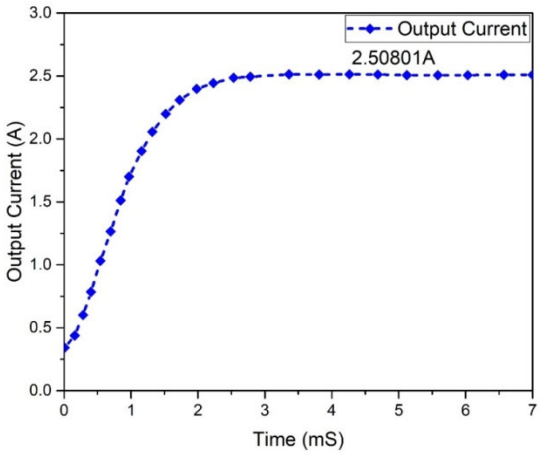

Figure 13. Output current of presented boost converter.

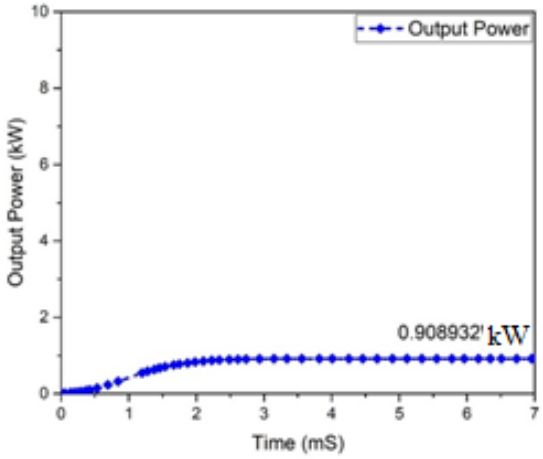

Figure 14. Output power of proposed boost converter.

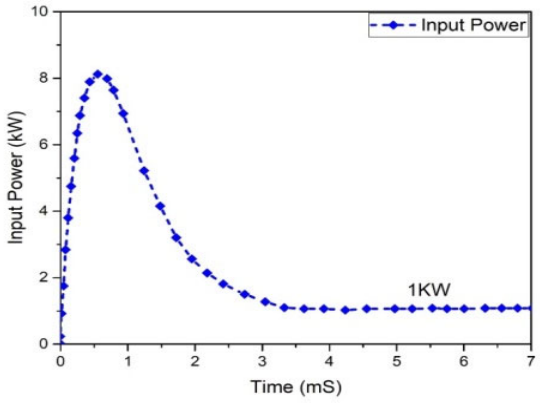

Figure 15. Boost converter input power.

Figure 16 depicts the output voltage performance of the suggested interleaved boost converter, which had a value of 362.886 V. The graph of the output current behavior of an interleaved boost converter is revealed in Figure 17, which shows a current of 2.51 A, while the estimated wind was 2.63 A. The input and output power waveforms of the interleaved boost converter are declared in Figures 18 and 19, which exhibit a 911.403 W input power and a 1 KW output power, respectively.

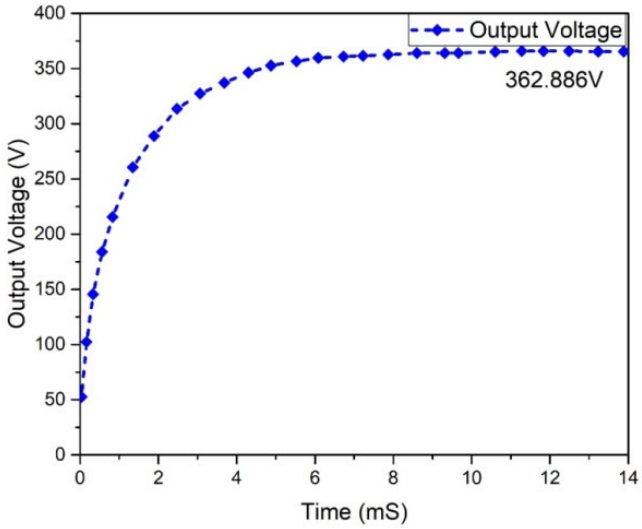

Figure 16. Results analysis of output voltage of interleaved boost converter.

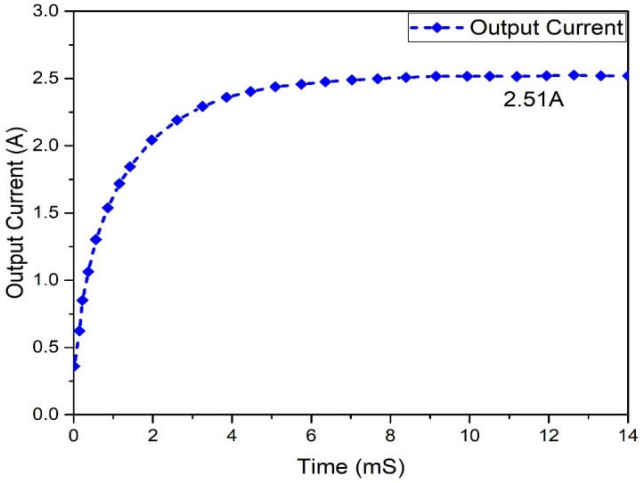

Figure 17. Results analysis of output current of interleaved boost converter.

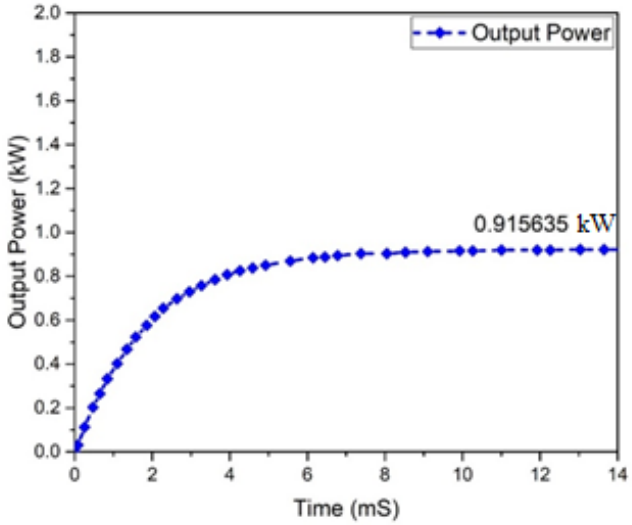

Figure 18. Output power of interleaved boost converter.

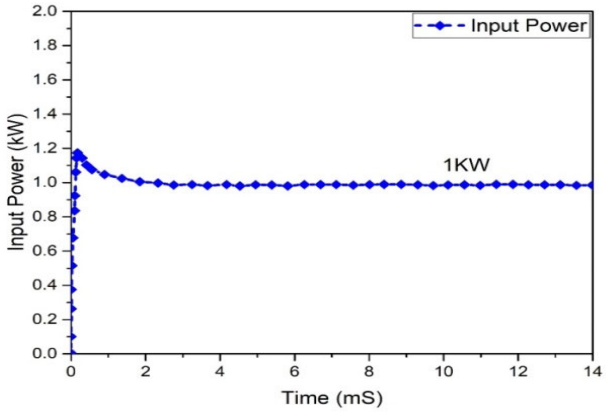

Figure 19. Input power analysis of interleaved boost converter.

The experimental analysis of the Flyback-Based converter (GaN HEMT) is presented in Figure 20, which reveals the behavior of the output voltage. Figures 21 and 22 illustrate the circuit's power based on GaN-HEMT after the voltage is raised using a Flyback boost converter.

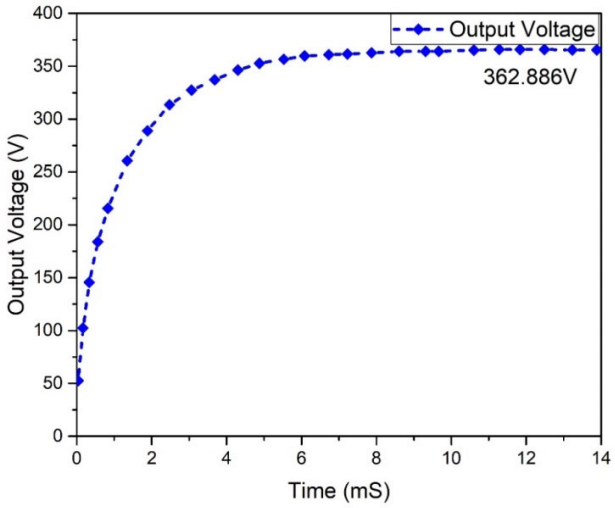

Figure 20. Output voltage of presented Flyback boost converter based (GaN-HEMT).

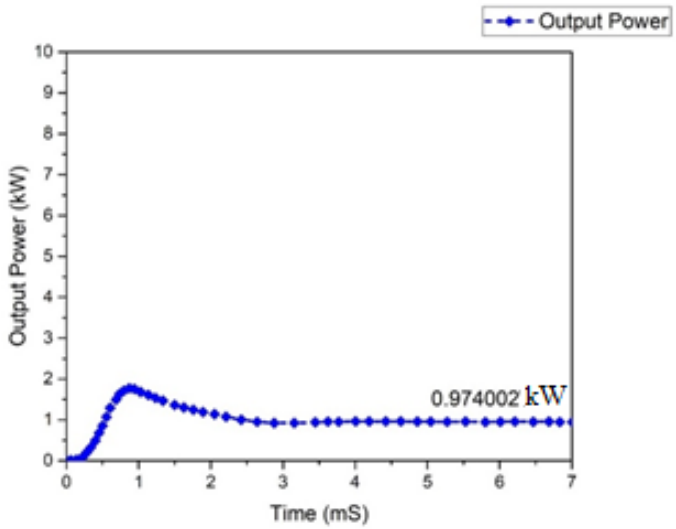

Figure 21. Output power of Flyback boost converter based (GaN-HEMT).

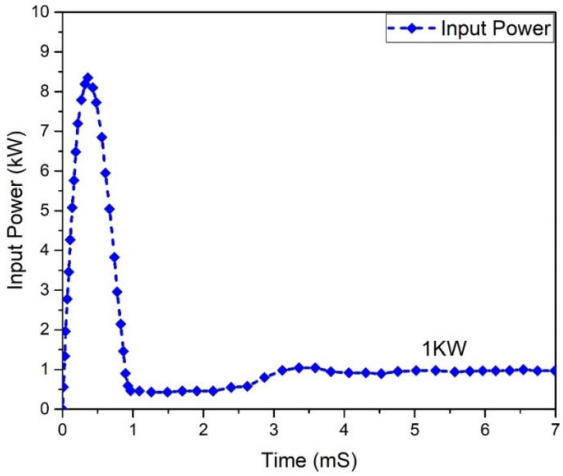

Figure 22. Input power of Flyback boost converter (GaN-HEMT).

One of the most significant characteristics of any converter is its efficiency. All power-processing applications necessitate high-efficiency converters. It is unfeasible to construct a converter if it demonstrates a lower efficiency. In a steady condition, the waveforms of the input power and output of the Flyback boost converter can be seen in Figures 23 and 24. As indicated, the value of the input power was 1 kW. In comparison, the output power was raised to 0.950555 kW for the mentioned input.

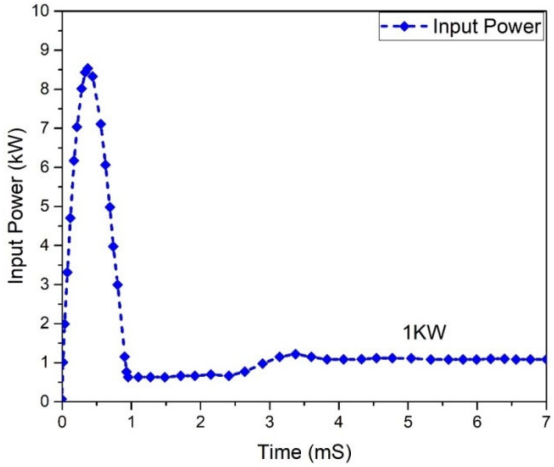

Figure 23. Input power of Flyback boost converter (Si-MOSFET).

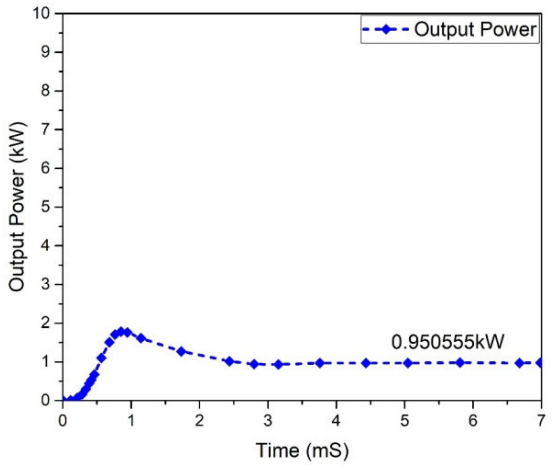

Figure 24. Output Power of Flyback boost converter (Si-MOSFET).

The Flyback-based converter's efficiency is estimated as

$$\eta = \frac{Output\ Power}{Input\ Power} = 0.950555 = 95\% \tag{49}$$

At this stage of operation, Modes 3 and 1 are observed, and it has been found that in the case of the Flyback boost converter, the value of the peak voltage crosswise the MOSFET appears. The MOSFETs used in the converter must tolerate the high peak voltages. MOSFET voltage waveforms are shown in Figure 25. The Flyback-based converter represents the voltage stress of 151.284 V across all MOSFETs. In a Flyback-based converter, the maximum current via a MOSFET occurs in Modes 1 and 3. This is significant because the MOSFETs used in the converter must withstand the maximum current stress. Current stress waveforms in MOSFETs are shown in Figure 26. It shows that each MOSFET has the current stress of 10.310 A.

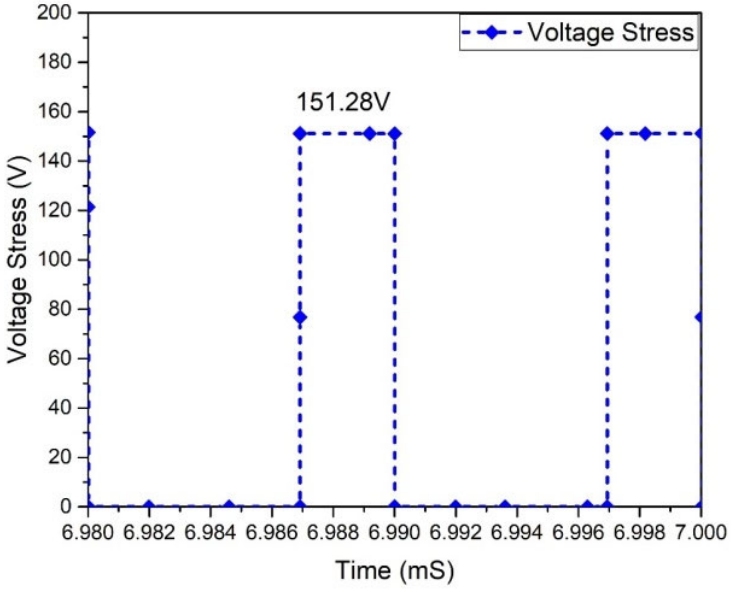

Figure 25. Voltage stress of MOSFETs.

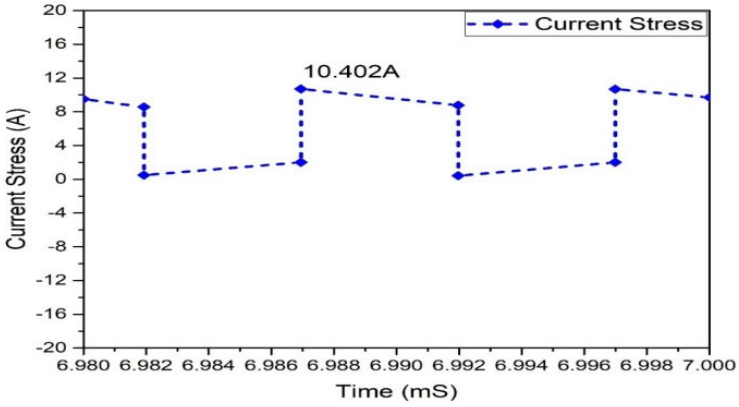

Figure 26. Current stress of MOSFETs.

All power-processing applications necessitate the use of high-efficiency converters. When a converter's efficiency is low, creating one is impractical. The graphs of the input and output power behavior for a (GaN HEMT) based Flyback-based converter are shown in Figures 27 and 28. According to the table below, the input power value is noted to be 1.0 kW, and the value of the power at the output is 974.002 W.

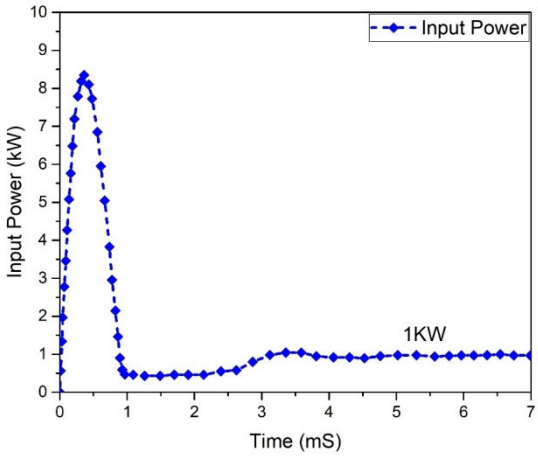

Figure 27. Input power (GaN-HEMT).

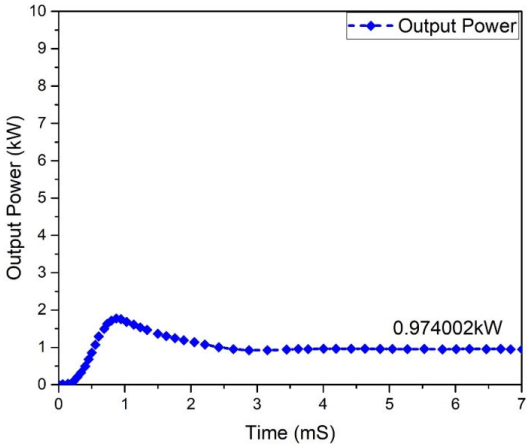

Figure 28. Output power (GaN-HEMT).

The Flyback-based converter based (GaN-HEMT) has the following efficiency:

$$\eta = \frac{Output\ Power}{Input\ Power} = 0.974002 = 97\% \tag{50}$$

In the operational stage in Modes 1 and 3 of a Flyback-boost converter, the maximum voltage is passed across the HEMT; thus, the HEMTs converters must be able to tolerate peak voltages. Voltage waveforms of HEMTs are shown in Figure 29, which offers a voltage stress of 150 V across all HEMTs in the Flyback-based converter.

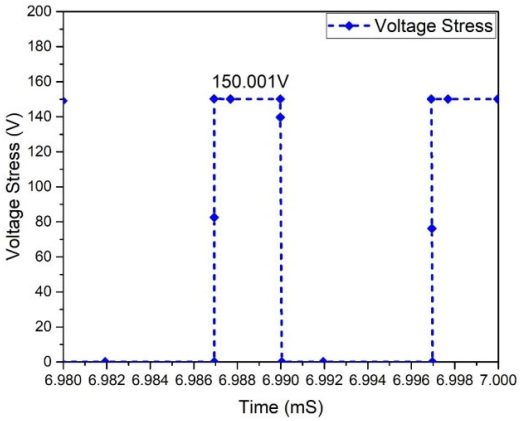

Figure 29. Voltage stress of HEMT.

In a Flyback-based (GaN-HEMT) boost converter, the maximum current via a HEMT occurs in Modes 1 and 3. This is significant because the HEMT used in the converter must withstand the maximum current stress. Waveforms of current strains in HEMT are shown in Figure 30. The current stress in each HEMT is 10 A, according to the data.

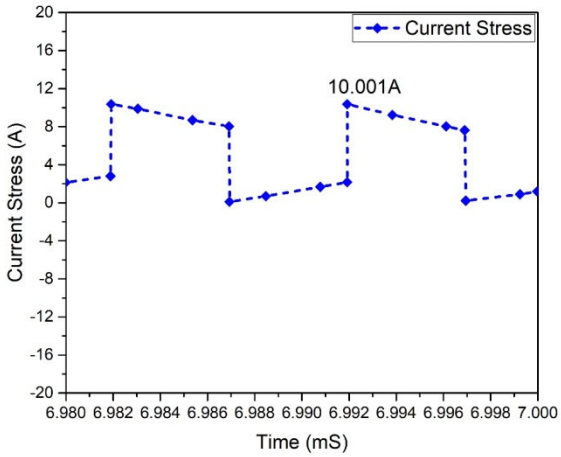

Figure 30. Current stress of HEMT.

Table 2 explains the relations among the Flyback Si-MOSFET converter, boost Si-MOSFET converter, interleaved boost Si-MOSFET converter, and Flyback boost GaN-HEMT in terms of efficiency, voltage stress, and current stress. This shows that the efficiencies of the proposed Flyback boost GaN-HEMT converter and the Flyback Si-MOSFT converter are better than current approached. The correlation of the presented work with the current system is depicted in Table 3, which explains the optimum solutions of the proposed system as compared to current models.

Table 3. Comparison of the proposed model with current approaches.

Description	[40]	[41]	[42]	This Work
Efficiency	95	94	95.5	97
Voltage stress (V)	380	380	376	152
Current stress (A)	20	19.5	19	11
Voltage gain (G)	(3-d1-d2)/(1-d1-d2)	4/1-d1	4/1-d1	D1/1-D1
Diodes	4	3	3	2
Switches	4	3	2	2
Inductors	3	4	3	2
Capacitors	4	3	2	1

5. Conclusions

In this study, three DC–DC converters were investigated for a higher power and lower voltages in power systems based on renewable energy: Flyback-based converter, Interleaved boost converter, and standard Boost converter. In a system that is a combination of the tacked fuel cells and PV arrays modules, the low voltages are boosted to 380.00 V, and the nature of voltage is DC, which is essential for a complete bridge inverter for the creation of 220 V having the nature of AC to be interfaced to the 220.00 V AC grid. Utilizing the setup of PSpice, the converters have been developed. The simulation has been carried out, selecting the proposed technologies to analyze the selection of the best technology and model. High-voltage conversion ratios are used in the converters. Additionally, the only better circuit to be used is to improve the production quality and thus the efficiency of the renewable energy systems. That has dramatically brought a change. It has become

possible because of the availability of the converters consisting of a high efficiency and connecting the resources of renewable energies to the grid-connected power system running on 220 V AC. Consumer demand for electricity varies greatly. When a renewable energy system is connected directly to consumers rather than through a grid, it is not easy to operate properly. Because of the fluctuating nature of consumer load, this is the case. According to the simulation results, the Flyback-based converter is the best choice for connecting stacked fuel cell and PV arrays modules (lower voltages) to the grid of 220.00 V AC. In this case, the main component used is the inverter that converts DC to AC. In short, the Flyback-based converter has the best topology with a higher efficiency, minimal stress of the device, and higher switching frequency. Additionally, GaN-based technology is the most effective way to boost converter efficiency.

In the present research work, the two technologies, i.e., Si-MOSFET- and GaN-HEMT-based converters, were studied. This study can be extended by considering SiC-MOSFET-based converters. The proposed GaN-HEMT-based boost converters can be further investigated for electric and hybrid vehicles.

Author Contributions: Conceptualization, F.A., K.S. and A.A.; methodology, A.A. and A.A.A.A.; software, F.A. and A.-S.M.; validation, M.A.; formal analysis, A.A.A.A.; investigation, K.S., A.A.A.A. and A.-S.M.; resources, M.A.; data curation, A.-S.M.; writing—original draft preparation, K.S.; writing—review and editing, F.A. and N.U.; visualization, N.U.; supervision, F.A. and N.U.; project administration, M.A.; funding acquisition, A.A., N.U. and A.A.A.A. All authors have read and agreed to the published version of the manuscript.

Funding: This research was supported by the Taif University Researchers Supporting Project number (TURSP-2020/144), Taif University, Taif, Saudi Arabia.

Institutional Review Board Statement: Not Applicable.

Informed Consent Statement: Not Applicable.

Data Availability Statement: The data is available in the paper.

Conflicts of Interest: The authors declare no conflict of interest.

References

1. Islam, M.S.; Jahid, A.; Islam, A.S.M.T.; Sharif; Sadath, M.A.; Monju, M.K.H. Renewable energy aware cost assessment for green data center with hybrid energy sources. In Proceedings of the 1st International Conference on Robotics, Electrical and Signal Processing Techniques, ICREST 2019, Dhaka, Bangladesh, 10–12 January 2019; pp. 120–125. [CrossRef]
2. Miao, S.; Wang, F.; Ma, X. A New Transformerless Buck-Boost Converter With Positive Output Voltage. *IEEE Trans. Ind. Electron.* **2016**, *63*, 2965–2975. [CrossRef]
3. Haseeb, I.; Armghan, A.; Khan, W.; Alenezi, F.; Alnaim, N.; Ali, F.; Muhammad, F.; Albogamy, F.R.; Ullah, N. Solar Power System Assessments Using ANN and Hybrid Boost Converter Based MPPT Algorithm. *Appl. Sci.* **2021**, *11*, 11332. [CrossRef]
4. Mohseni, P.; Rahimpour, S.; Dezhbord, M.; Islam, M.R.; Muttaqi, K.M. An Optimal Structure for High Step-Up Nonisolated DC–DC Converters With Soft-Switching Capability and Zero Input Current Ripple. *IEEE Trans. Ind. Electron.* **2022**, *69*, 4676–4686. [CrossRef]
5. Mohseni, P.; Hosseini, S.H.; Sabahi, M.; Jalilzadeh, T.; Maalandish, M. A new high step-up multi-input multi-output DC–DC converter. *IEEE Trans. Ind. Electron.* **2019**, *66*, 5197–5208. [CrossRef]
6. Islam, M.R.; Mahfuz-Ur-Rahman, A.M.; Islam, M.M.; Guo, Y.G.; Zhu, J.G. Modular medium-voltage grid-connected converter with improved switching techniques for solar photovoltaic systems. *IEEE Trans. Ind. Electron.* **2017**, *64*, 8887–8896. [CrossRef]
7. Chen, Y.T.; Lin, W.C.; Liang, R.H. An interleaved high step-up DC–DC converter with double boost paths. *Int. J. Circuit Theory Appl.* **2015**, *43*, 967–983. [CrossRef]
8. Kumar, G.B.A. Shivashankar Optimal power point tracking of solar and wind energy in a hybrid wind solar energy system. *Int. J. Energy Environ. Eng.* **2021**, *13*, 77–103. [CrossRef]
9. Forouzesh, M.; Shen, Y.; Yari, K.; Siwakoti, Y.P.; Blaabjerg, F. High-efficiency high step-up DC–DC converter with dual coupled inductors for grid-connected photovoltaic systems. *IEEE Trans. Power Electron.* **2018**, *33*, 5967–5982. [CrossRef]
10. Marzang, V.; Tabbat, P.A.; Khoshkbar-Sadigh, A.; Mohseni, P.; Hashemzadeh, S.M.; Talebian, I. An interleaved high step-up DC–DC converter with low voltage-stress on semiconductors. In Proceedings of the IECON 2020 The 46th Annual Conference of the IEEE Industrial Electronics Society, Singapore, 18–21 October 2020; pp. 1223–1228.
11. Qi, Q.; Ghaderi, D.; Guerrero, J.M. Sliding mode controller-based switched-capacitor-based high DC gain and low voltage stress DC–DC boost converter for photovoltaic applications. *Int. J. Electr. Power Energy Syst.* **2021**, *125*, 106496. [CrossRef]

12. Hassan, W.; Hasan, R.; Lu, D.D.; Xiao, W. Design and Development of High Step-up DC–DC Converter to Realize High Efficiency and Reduced Voltage Stress. In Proceedings of the Applied Power Electronics Conference and Exposition (APEC) 2020 IEEE, New Orleans, LA, USA, 15–19 March 2020; pp. 2098–2103.
13. Hassan, W.; Soon, J.L.; Gautam, S.; Lu, D.D.; Xiao, W. Optimized Coupled Inductor DC/DC Converter by Integrating Snubber Circuit with Voltage Lift Technique. In Proceedings of the Industrial Electronics Society (IECON) 2020 The 46th Annual Conference of the IEEE, Singapore, 18–21 October 2020; pp. 1401–1405.
14. Kumar, G.K.; Elangovan, D.; Arunkumar, G. Multiple Input Interleaved Boost Converter for Non-Conventional Energy Applications. In Proceedings of the Innovations in Power and Advanced Computing Technologies (i-PACT) 2019, Vellore, India, 22–23 March 2019; Volume 1, pp. 1–5.
15. Pala, V.; Peng, H.; Wright, P.; Hella, M.M.; Chow, T.P. Integrated high-frequency power converters based on GaAs pHEMT: Technology characterization and design examples. *IEEE Trans. Power Electron.* **2012**, *27*, 2644–2656. [CrossRef]
16. Abeta, H.; Obara, H.; Kawamura, A. Multiple Source Input Isolated DC-DC Converter with Simple Circuit. *IEEJ Trans. Ind. Appl.* **2019**, *139*, 266. [CrossRef]
17. Netzahuatl, E.; Cortes, D.; Ramirez-Salinas, M.A.; Resa, J.; Hernandez, L.; Hernandez, F.-D. Modeling Design Procedure and Control of a Low-Cost High-Gain Multi-Input Step-Up Converter. *Electronics* **2019**, *8*, 1424. [CrossRef]
18. Spiazzi, G.; Mattavelli, P.; Gazoli, J.R.; Magalhaes, R.; Frattini, G. Improved integrated boost-flyback high step-up converter. In Proceedings of the IEEE International Conference on Industrial Technology, Via del Mar, Chile, 14–17 March 2010; pp. 1169–1174. [CrossRef]
19. Kumar, C.P.; Venugopal, N. Performance and Stability Analysis of Series-Cascaded High-Gain Interleaved Boost Converter for Photovoltaic Applications. *Power Electron. Drives* **2018**, *3*, 85. [CrossRef]
20. Wu, H.; Xia, T.; Zhan, X.; Xu, P.; Xing, Y. Resonant converter with resonant-voltage-multiplier rectifier and constant frequency phase-shift control for isolated buck–boost power conversion. *IEEE Trans. Ind. Electron.* **2015**, *62*, 6974–6985. [CrossRef]
21. Ramanathan, G.G.; Urasaki, N. Non-Isolated Interleaved Hybrid Boost Converter for Renewable Energy Applications. *Energies* **2022**, *15*, 610. [CrossRef]
22. Hu, X.; Wang, J.; Li, L.; Li, Y. A Three-Winding Coupled-Inductor DC–DC Converter Topology with High Voltage Gain and Reduced Switch Stress. *IEEE Trans. Power Electron.* **2018**, *33*, 1453–1462. [CrossRef]
23. Vecchia, M.D.; Salvador, M.A.; Lazzarin, T.B. Hybrid Nonisolated DC–DC Converters Derived From a Passive Switched-Capacitor Cell. *IEEE Trans. Power Electron.* **2018**, *33*, 3157–3168. [CrossRef]
24. Martinez-Lopez, M.; Moreno-Valenzuela, J.; He, W. A robust nonlinear PI-type controller for the DC–DC buck–boost power converter. *ISA Trans.* 2022; *in press*. [CrossRef]
25. Ma, W.; Zhang, B.; Qiu, D.; Sun, H. Switching Control Strategy for DC–DC Converters Based on Polynomial Lyapunov Function and Sum-of-Squares Approach. *IEEE Trans. Ind. Electron.* **2022**. [CrossRef]
26. Erickson, R.W.; Maksimovic, D. *Fundamental of Power Electronics*; Kluwer: Norwell, MA, USA, 2001; pp. 589–630.
27. Premkumar, M.; Karthick, K.; Sowmya, R. A comparative study and analysis on conventional solar pv based DC–DC converters and MPPT techniques. *Indones J. Electr. Eng. Comput. Sci.* **2018**, *11*, 831–838.
28. Nouri, T.; Vosoughi, N.; Hosseini, S.H.; Babaei, E.; Sabahi, M. An Interleaved High Step-Up Converter With Coupled Inductor and Built-In Transformer Voltage Multiplier Cell Techniques. *Ind. Electron. IEEE Trans.* **2019**, *66*, 1894–1905. [CrossRef]
29. Andrade, A.M.S.S.; Schuch, L.; da Silva Martins, M.L. Analysis and Design of High-Efficiency Hybrid High Step-Up DC–DC Converter for Distributed PV Generation Systems. *Ind. Electron. IEEE Trans.* **2019**, *66*, 3860–3868. [CrossRef]
30. Varesi, K.; Hosseini, S.H.; Sabahi, M.; Babaei, E.; Saeidabadi, S.; Vosoughi, N. Design and Analysis of a Developed Multiport High Step-Up DC–DC Converter with Reduced Device Count and Normalized Peak Inverse Voltage on the Switches/Diodes. *Power Electron. IEEE Trans.* **2019**, *34*, 5464–5475. [CrossRef]
31. Kumar, N.; Veerachary, M. Stability Region Based Robust Controller Design for High-Gain Boost DC–DC Converter. *Ind. Electron. IEEE Trans.* **2021**, *68*, 2246–2256. [CrossRef]
32. Chen, H.; Hu, X.; Huang, Y.; Zhang, M.; Gao, B. Improved DC–DC converter topology for high step-up applications. *IET Circuits Devices Syst.* **2018**, *13*, 51–60. [CrossRef]
33. Saadatizadeh, Z.; Heris, P.C.; Babaei, E.; Sadikoglu, F. Expandable interleaved high voltage gain boost DC–DC converter with low switching stress. *Int. J. Circuit Theory Appl.* **2019**, *47*, 782–804. [CrossRef]
34. Ravindra, S.; Reddy, A.N.; Tejaswi, K.N.V.S.; Shamili, K.B. Comparative Analysis of MPPT Techniques Using DC–DC Converter Topologies for PV Systems. In *DC–DC Converters for Future Renewable Energy Systems*; Energy Systems in Electrical Engineering; Priyadarshi, N., Bhoi, A.K., Bansal, R.C., Kalam, A., Eds.; Springer: Singapore, 2022. [CrossRef]
35. Tseng, K.-C.; Chen, J.-Z.; Lin, J.-T.; Huang, C.-C.; Yen, T.-H. High Step-Up Interleaved Forward-Flyback Boost Converter With Three-Winding Coupled Inductors. *Power Electron. IEEE Trans.* **2015**, *30*, 4696–4703. [CrossRef]
36. Balaji, P.; Kowsalya, M. Design a high-efficiency and high voltage gain DC-DC converter for photo voltaic systems. In Proceedings of the 2017 International Conference on Communication and Signal Processing (ICCSP), Chennai, India, 6–8 April 2017; pp. 1729–1733.
37. Tseng, K.-C.; Cheng, C.-A.; Chen, C.-T. High Step-Up Interleaved Boost Converter for Distributed Generation Using Renewable and Alternative Power Sources. *Emerg. Sel. Top. Power Electron. IEEE J.* **2017**, *5*, 713–722. [CrossRef]

38. Amir, A.; Amir, A.; Che, H.S.; Elkhateb, A.; Rahim, N.A. Comparative analysis of high voltage gain DC–DC coverter topologies for photovoltaic systems. *Renew. Energy* **2019**, *136*, 1147–1163. [CrossRef]
39. Shayeghi, H.; Pourjafar, S.; Hashemzadeh, S.M.; Sedaghati, F. Presenting of the Magnetic Coupling-Based Transformer-Less High Step-Up DC-DC Converter for Renewable Energy Applications. *Int. Trans. Electr. Energy Syst.* **2022**, *2022*, 3141119. [CrossRef]
40. Shojaeian, H.; Heydari, M.; Hasanzadeh, S. Improved interleaved high step-up converter with high efficiency for renewable energy applications. In Proceedings of the 2017 8th Power Electronics Drive Systems & Technologies Conference (PEDSTC), Mashhad, Iran, 14–16 February 2017; pp. 288–293.
41. Ali, A.; Ullah, R.; Ullah, Z. DC-to-DC converters for low-voltage high-power renewable energy systems. *World Acad. Sci. Eng. Technol. Int. J. Electr. Comput. Energetic Electron. Commun. Eng.* **2015**, *9*, 1299–1304.
42. Waqas, H.; Lu, D.; Xiao, W. Optimal analysis and design of DC-DC converter to achieve high voltage conversion gain and high efficiency for renewable energy systems. In Proceedings of the 2018 IEEE 27th International Symposium on Industrial Electronics (ISIE), Cairns, Australia, 13–15 June 2018.